Pergamon

0967-0637(94)E0002-9

Deep-Sea Research I, Vol. 41, No. 8, pp. 1207–1229, 1994

0967-0637/94 $7.00 + 0.00

Alignment of lenses: laboratory and numerical experiments

DORON NOF* and W. K. DEWAR†

(*Received* 13 *May* 1993; *in revised form* 30 *November* 1993; *accepted* 27 *December* 1993)

Abstract—This paper addresses the question of what happens when two anticyclonic lens-like eddies with different densities come in contact with each other by, say, an advective current. We use laboratory and numerical experiments to demonstrate that, in a similar fashion to lenses with identical densities which often merge, lenses with unequal densities often *align* (i.e. the lenses "strive" toward a state where one lens is situated on top of the other). The two initially isolated eddies are formed in the laboratory by continuously injecting salty water through small filters situated in the interface separating two environmental layers. Hence, there is a total of four different fluids with graduated densities in the tank. The heaviest water is the lowest layer. One of the lenses is slightly lighter than this heaviest water and the other is still lighter than the first lens. Finally, the upper layer is the lightest of the four. Since the lenses are formed by injection, weak anticyclones which extend beyond the boundary of the lenses are formed above and below the lenses.

Due to the continuous injection of fluid into the lenses they grow slowly so that after some time their edges meet. As in merging of lenses with identical densities, arms are then extended from one vortex to the other. However, in the present case the arms are situated above the heavier vortex and below the lighter vortex instead of being at the same level. At this point, the lenses are locked together and the arms continue to propagate and grow until the lenses ultimately align. This process is accompanied by filamentation where fluid is expelled from both lenses to accommodate the change in angular momentum.

Comparable numerical experiments also are discussed. Here Gaussian lenses in a four-layer fluid are studied; the lenses occupy the two intermediate layers. The physical parameters of these experiments are chosen to resemble the now famous case of observed eddy merging off East Australia. In contrast to the laboratory study, the numerical lenses have no initial anticyclones located in the layers surrounding them. The results indicate alignment in a manner similar to the laboratory experiments, provided the eddies are initially sufficiently close.

1. INTRODUCTION

(a) *Background*

THE question of how eddies merge and break up in the ocean is important because of the associated transfer of energy and heat from small to large scale and vice versa.

The first observations of eddy merging were made by CRESSWELL (1982) (Fig. 1a) off East Australia [see also CRESSWELL and LEGECKIS (1987)], followed by ROBINSON *et al.* (1986) who observed merger in the eastern Pacific. More recently, it has been recognized

*Department of Oceanography and the Geophysical Fluid Dynamics Institute, Florida State University, Tallahassee, FL 32306-3048, U.S.A.

†Department of Oceanography, Geophysical Fluid Dynamics Institute, and Supercomputer Computations Research Institute Florida State University, Tallahassee, FL 32306-3048, U.S.A.

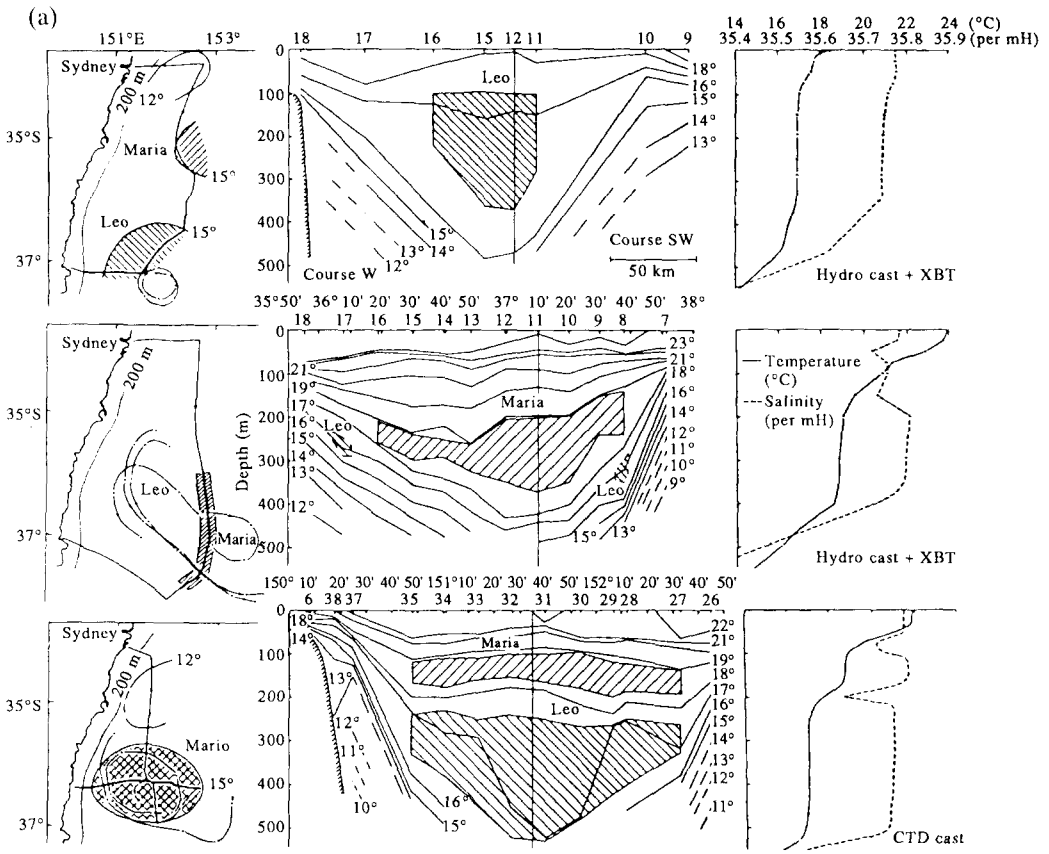
(a)
151°E
153°
Sydney
200 m
12°
35°S
Maria
15°
Leo
15°
37°
18 17 16 15 12 11 10 9
Leo
18°
16°
15°
14°
13°
100
200
300
400
500
15°
13° 14°
12°
Course W
Course SW
50 km
14 16 18 20 22 24 (°C)
35.4 35.5 35.6 35.7 35.8 35.9 (per mH)
Hydro cast + XBT
35°50' 36° 10' 20' 30' 40' 50' 37° 10' 20' 30' 40' 50' 38°
18 17 16 15 14 13 12 11 10 9 8 7
Sydney
200 m
35°S
Depth (m)
Maria
Leo
Leo
Maria
37°
23°
21°
19°
17°
16°
15°
14°
13°
12°
18°
16°
14°
12°
11°
10°
9°
15° 13°
Temperature (°C)
Salinity (per mH)
Hydro cast + XBT
150° 10' 20' 30' 40' 50' 151°10' 20' 30' 40' 50' 152°10' 20' 30' 40' 50'
6 38 37 35 34 33 32 31 30 29 28 27 26
Sydney
200 m
12°
35°S
Mario
15°
37°
18°
14°
13°
12°
11°
10°
Maria
Leo
22°
21°
19°
18°
17°
16°
15°
14°
13°
12°
11°
16°
15°
CTD cast

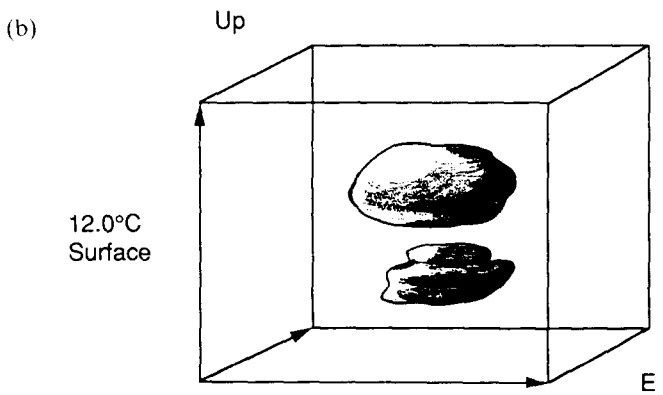
(b)
Up
12.0°C
Surface
E

that the eddies formed in the Mediterranean outflow (i.e. Meddies) often occur in a so-called double-core state (Fig. 1b) that resembles the merged state seen by Cresswell (see e.g. RICHARDSON *et al.*, 1989, p. 378). On the basis of Cresswell's observations (Fig. 1a), GILL and GRIFFITHS (1981) pointed out, in a short and informal note, that, if the two lenses with identical densities conserve their mass and potential vorticity during the merging, then an additional source of energy must be supplied to complete the process. This informal note had a rather large impact on the field, and, subsequently, many investigators have been attracted to the merging process (see e.g. GRIFFITHS and HOPFINGER, 1986, 1987; MCWILLIAMS and ZABUSKY, 1982; MELANDER *et al.*, 1985, 1987, 1988; NOF and SIMON, 1987; NOF, 1988).

These investigators have mainly focused on the merging conditions and tried to resolve the energy paradox. Suggestions for the paradox resolution have ranged from the idea that the additional necessary energy is supplied by the flow above or below the eddies to concepts which consider alteration of the potential vorticity during the merging. Although both of these processes are theoretically possible, neither is very appealing. A more sensible resolution of the energy issue was later provided by CUSHMAN-ROISIN (1989) who showed that an ejection of mass via filamentation can resolve the energy question. The energy question was later revisited by POLVANI *et al.* (1989) who showed that filamentation of quasi-geostrophic eddies is suppressed by a very deep lower layer, and by DEWAR and KILLWORTH (1990) who argued that mixing of potential vorticity *outside* the eddies also can resolve the paradox.

All of the above studies have focused on linear quasi-geostrophic eddies as well as nonlinear eddies with *identical* densities. However, as can be seen in Cresswell's data, the participant eddies were clearly of different densities, and one eddy apparently "climbed" on top of its counterpart during the interaction. Further, although the formation of double-core Meddies has not been observed, their relatively frequent appearance argues that a powerful mechanism exists to join the cores, each of which resides on a distinct isopycnal. The purpose of our present study is to bring the theoretical analysis closer to the observations by considering the interaction of two eddies of different rather than identical densities. The difference between the two cases is not at all trivial, as stratification is known to drastically decrease the tendency of eddies to merge (e.g. MASINA and PINARDI, 1993). Hence, it is not *a priori* obvious that eddies with different densities will even have a *tendency* to unite. It is appropriate to refer to our process of eddies (with different densities) fusion as *alignment* rather than merging because the fluids of the eddies do not mix. This was recognized by MCWILLIAMS (1989) who modeled eddies using quasi-

Fig. 1.(a) The alignment of two anticyclonic eddies off East Australia (adapted from CRESSWELL, 1982). The results of Cresswell's ship surveys for December 1980, January 1981 and April 1981 are shown on top, middle and bottom, (respectively). In column 1 buoy tracks for several days before and after the surveys are marked; regions having 250-m temperatures exceeding 15°C are shaded; the 12°C isotherm for 250 m is marked. The thickened ship tracks define the temperature sections (in degrees Celsius) in column 2 where the signature layers of eddies Leo and Maria are shaded. The vertical lines in column 2 indicate the positions for the temperature and salinity profiles of column 3. Note that Leo was heavier than Maria both before and after the alignment. (b) A three-dimensional perspective plot of a double-core Meddy. The Meddy dimensions are roughly 35 km by 35 km by 900 m (adapted from AMBAR *et al.*, 1992). Note that, since the Mediterranean Undercurrent itself usually has a double-core signature, the associated formation process is probably not identical to that of Fig. 1a. Nevertheless, this observation and others like it are indicative of the aligned state stabilities properties.

geostrophic theory and used the term "alignment" for the first time. With the aid of contour dynamics techniques, Polvani (1991) also examined *quasi-geostrophic* alignment. He argues that the tendency of eddies to align is related to the known baroclinic-to-barotropic energy cascade.

Here we consider the alignment of highly nonlinear eddies (i.e. lenses), which are, in a way, more closely related to actual oceanic eddies than McWilliams' and Polvani's quasi-geostrophic (i.e. small amplitude) eddies. Our aim is to determine the influence of nonlinearity on the alignment and to look at the problem from a different point of view, i.e. use laboratory experiments and primitive equation numerical modeling instead of contour dynamics. We shall see that, although our nonlinear computation is more applicable to the ocean than is linear theory, much of the dynamics also can be explained by quasi-geostrophic dynamics.

(b) *Experimental apparatus*

When fluid is injected at a point situated on the interface separating two layers with different densities, a lens is formed. To examine the interaction of two such lenses (each having a different density) they are formed in a way that they do not touch initially each other. Specifically, the distance between the two injection points is greater than the initial local Rossby radius (based on the lens depth) so that the initial lenses are well separated from each other. The injection is not terminated at any point so that the lenses grow and, ultimately, their edges meet. A complex interaction begins and it is this stage that is the focus of our experiment. The following apparatus was designed in order to allow a clear observation of this phenomenon.

A cylindrical Plexiglass tank, with an inner diameter of 45 cm and a height of about 45 cm, was mounted on a rotating table (Fig. 2). Two narrow tubes with small cylindrical permeable foams at their edges were inserted through the clear Plexiglass top. The experiments were performed on a variable speed rotating table and photographed with the aid of two 35 mm motor driven cameras. One was fixed to the rotating table and viewed the experiments from the top, while the other was fixed to the floor and viewed the experiments from the side. First, the tank was filled with the heaviest salty water to a height of about 11 cm. Then the second, somewhat lighter, fluid was slowly poured (via a permeable foam) over the first layer to form the 11 cm thick second layer. Afterwards, two lenses sandwiched between the two main layers were formed simultaneously by injecting fluids with intermediate densities.

The lenses' densities were as follows. The first lens had a density of $(\rho + \Delta\rho)$, where ρ is the density of the upper layer and $(\rho + 3\Delta\rho)$ is the density of the lower layer; the second lens had a density of $(\rho + 2\Delta\rho)$. We shall see later that this implies that the vertical separation between the lenses' centers of gravity was one sixth of a single lens total thickness.

(c) *Numerical procedures*

We also have conducted a series of numerical experiments using the isopycnal code originally described by BLECK and BOUDRA (1982), and which has been used in numerous subsequent studies (see e.g. CHASSIGNET and CUSHMAN-ROISIN, 1991; DEWAR and GAILLIARD, 1993). This is a primitive equation model that solves the equations:

$$\frac{\partial \mathbf{u}}{\partial t} + \nabla \cdot (\mathbf{u} \cdot \mathbf{u}/2) + \xi k \times \mathbf{u} = -\nabla \mathrm{M} + \frac{\nu}{h} \nabla \cdot h \nabla \mathbf{u}, \tag{1.1}$$

$$\frac{\partial}{\partial t} h + \nabla \cdot (h\mathbf{u}) = 0, \tag{1.2}$$

in each layer, where ξ is the absolute vorticity ($\xi = (\nabla x \mathbf{u}) \cdot \hat{k} + f$), M is the Montgomery potential ($\mathrm{M} = P/\rho + gz$) and the other notation is standard. We employ a four-layer implementation of the model, where the total depth is 4000 m. The upper and lower layers were taken to be 1990 m in thickness away from the lenses. Gaussian thickness profiles were provided to the second and third layers and equal density defects were assigned to all interfaces. Our standard experiment involved eddies with thicknesses of $h_{\mathrm{m}} = 450$ m. The deformation radii on this thickness and our density defects were:

$$\sqrt{g' h_{\mathrm{m}}}/f_0 \cong 25 \text{ km}.$$

The Gaussian thickness profiles:

$$h_{\mathrm{i}} = h_{\infty \mathrm{i}} + \delta h_{\mathrm{i}} \, \mathrm{e}^{-r^2/2r_0^2},$$

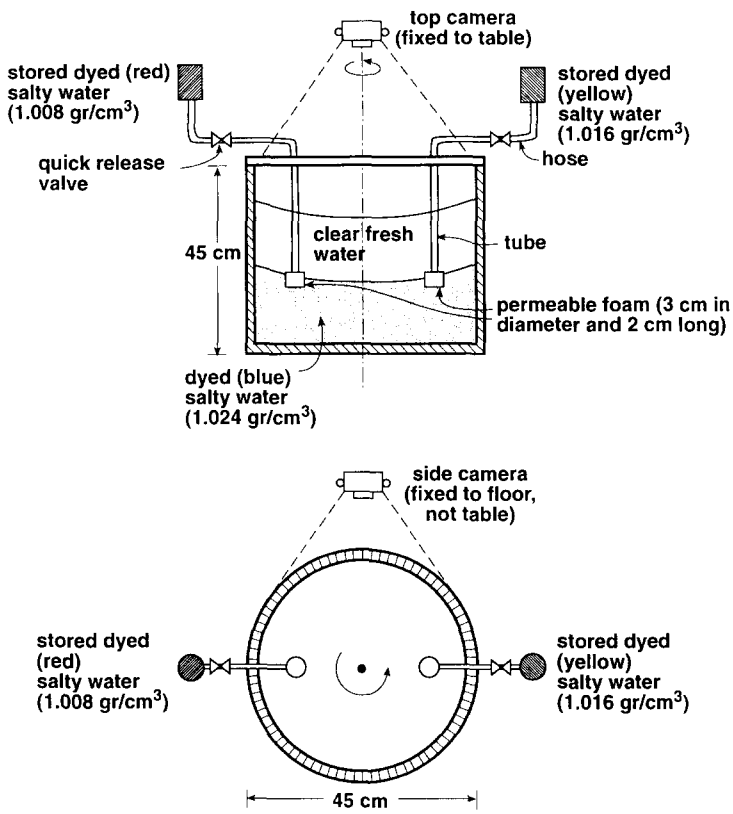

Fig. 2. A sketch of the experimental apparatus. The lenses are generated by continuously releasing stored fluids through the round permeable foams. After some time, the edges meet, a figure "8" structure is formed, arms are extended from one lens to the other and the lenses align.

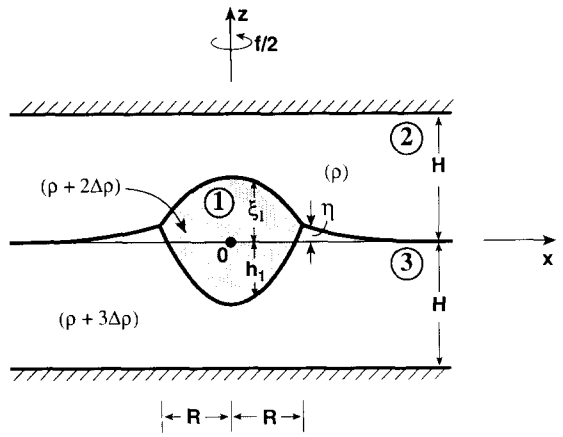

Fig. 3. Schematic diagram of an injection of fluid [with an intermediate density of $(\rho + 2\Delta\rho)$] along the interface separating a two-layer system whose densities are ρ and $(\rho + 3\Delta\rho)$. The injected fluid spreads horizontally away from the center so that a lens (i.e. an anticyclone) is formed. Due to divergence, anticyclones are also established above and below the lens. Although these anticyclones are weak, they extend much beyond the boundary of the lens (see text).

described here used $h_{\infty i} = 10$ m and $r_0 = 25$ km. This implies that in the initial numerical conditions the vertical separation is on the order of 10 m, much smaller than the one sixth thickness laboratory separation. Both vertical separations, however, are much smaller than the less vertical scale. This is in agreement with Cresswell's observations. The employed grid spacing was 4 km, time steps were 240 s, and the value of the viscosity was set to $\nu = 5 \times 10^5\ \mathrm{cm^2\,s^{-1}}$. We performed a series of experiments in which these parameters were varied, and have determined that the results reported here do not depend on them.

This paper is organized as follows. In section 2 we theoretically describe the formation of a lens in a laboratory tank. Namely, we describe the injection of fluid into a tank containing two fluids and the associated establishment of anticyclones above and below the lens.

2. SOME THEORETICAL CONSIDERATIONS

In what follows we shall present the velocity and pressure fields associated with a lens in a laboratory tank. Because both the upper and lower layer are of *finite* depth, flows are also generated above and below the lens and it is these eddies that we are presently interested in.

The solution presented below also may have direct application to oceanic eddies as such eddies are sometimes formed by processes similar to injection, see e.g. GILL (1981) who considered the injection of fluid into a stratified layer of infinite vertical extent. However, understanding all the mathematical details of the solution is not essential for the alignment process, and the reader who is not interested in the derivation may go directly to the results (2.52–2.55).

(a) *Governing equations*

We begin by considering the situation displayed in Fig. 3. Since the lens is formed by injection, there are initially large radical velocities and the time dependent terms cannot be

ignored. After some time, however, the lens becomes of sufficient size to permit neglecting the time-dependent terms. Namely, after some time the steady injection rate becomes small compared to the volume of the lens so that the lens growth rate is negligible and the problem can be treated as if it is steady. In this sense, the lens is similar to that formed by the collapse of a cylinder and the resulting adjustment process (e.g. NOF and SIMON, 1987; DEWAR and KILLWORTH, 1990).

For the above conditions, the momentum and potential vorticity equations for the lens and the layers above and below (i.e. $r \leq R$, where R is the radius of the lens) are,

$$\frac{v_2^2}{r} + fv_2 = \frac{1}{\rho}\frac{dp_2}{dr} \tag{2.1}$$

$$\frac{1}{r}\frac{r}{dr}(rv_2) = -\xi_1 \frac{f}{H} \tag{2.2}$$

$$\frac{v_1^2}{r} + fv_1 = \frac{1}{\rho}\frac{dp_2}{dr} + 2g'\frac{d\xi_1}{dr} \tag{2.3}$$

$$\frac{v_3^2}{r} + fv_3 = \frac{1}{\rho}\frac{dp_2}{dr} + 2g'\frac{d\xi_1}{dr} - g'\frac{dh_1}{dr} \tag{2.4}$$

$$\frac{1}{r}\frac{r}{dr}(rv_3) = -h_1 \frac{f}{H}, \tag{2.5}$$

where the subscripts 1, 2 and 3 correspond to the lens, the upper layer and the lower layer, (respectively), and p_2 and p_3 are the deviations of the upper and lower layer pressures from their motionless values, v_1, v_2 and v_3 are the orbital speeds, h_1 and ξ_1 are the displacements of the lower and upper lens interfaces from the undisturbed depth (measured downward and upward, respectively), f is the Coriolis parameter and H is the environmental layer undisturbed depth.

Since it is not *a priori* obvious what the potential vorticity of the lens is, it is necessary to look at the conservation of angular momentum $[(D/Dt)(rv_1 + fr^2/2) = 0]$. Assuming that the injection is done at a point ($r = 0$) and that $Lim_{r\to 0} rv_1 = 0$ (i.e. the angular momentum is zero), we immediately find that the velocity profile within the lens is,

$$v_1 = -fr/2, \tag{2.6}$$

because all of the lens fluid originates from the point source. It is easy to show that this solution essentially corresponds to a zero potential vorticity lens.

The governing equations for the regions outside the lens ($r \geq R$) are,

$$\frac{v_2^2}{r} + fv_2 = \frac{1}{\rho}\frac{dp_3}{dr} \tag{2.7}$$

$$\frac{1}{r}\frac{d}{dr}(rv_2) = -\eta \frac{f}{H} \tag{2.8}$$

$$\frac{v_3^2}{r} + fv_3 = \frac{1}{\rho}\frac{dp_3}{dr} + 3g'\frac{d\eta}{dr} \tag{2.9}$$

$$\frac{1}{r}\frac{d}{dr}(rv_3) = \eta \frac{f}{H}, \tag{2.10}$$

where η is the interface displacement (measured upward).

The radius of the lens R is assumed to be small compared to the Rossby radius (R_d) based on the environmental fluid depth.

$$R = \varepsilon^{1/2} R_d = \varepsilon^{1/2}(g'H)^{1/2}/f; \quad \varepsilon \ll 1. \tag{2.11}$$

In view of this, one finds that the appropriate scales are,

$$\left.\begin{aligned} &r \sim O(\varepsilon^{1/2} R_d);\ v_1 \sim O(\varepsilon^{1/2} f R_d);\ v_2, v_3 \sim O(\varepsilon^{3/2} f R_d) \\ &\xi_1 \sim O(\varepsilon H);\ h_1 \sim O(\varepsilon H);\ p_2 \sim O(\varepsilon^2 \rho f^2 R_d^2) \\ &\eta \sim O(\varepsilon^2 H);\ p_3 \sim O(\varepsilon^2 \rho f^2 R_d^2). \end{aligned}\right\} \tag{2.12}$$

In the limit of $\varepsilon \to 0$, the lens degenerates to a point. It will become clear later that because of this particular aspect, it is more convenient to initially scale the equations with the O(1) parameters. Namely, we define,

$$\left.\begin{aligned} &v_1^* = v_1/fR_d;\ v_2^* = v_2/fR_d;\ v_3^* = v_3/fR_d;\ r^* = r/R_d;\ h_1^* = h_1/H, \\ &\xi_1^* = \xi_1/H;\ p_2^* = p_2/f^2 R_d^2 \rho;\ p_3 f^2 R_d^2 \rho, \\ &\eta^* = \eta/H. \end{aligned}\right\} \tag{2.13}$$

In terms of these variables, the governing equations for $r \le R$ are,

$$\frac{(v_2^*)^2}{r^*} + v_2^* = \frac{dp_2^*}{dr^*} \tag{2.14}$$

$$\frac{1}{r^*}\frac{d}{dr^*}(r^* v_2^*) = -\xi_1^* \tag{2.15}$$

$$-\frac{r^*}{4} = \frac{dp_2^*}{dr^*} + 2\frac{d\xi_1^*}{dr^*} \tag{2.16}$$

$$\frac{(v_3^*)^2}{r^*} + v_3^* = \frac{dp_2^*}{dr^*} + 2\frac{d\xi_1^*}{dr^*} - \frac{dh_1^*}{dr^*} \tag{2.17}$$

$$\frac{1}{r^*}\frac{d}{dr^*}(r^* v_3^*) = -h_1^*, \tag{2.18}$$

where (2.6) has been combined with (2.3).

Similarly, for $r \ge R$ the equations are,

$$\frac{(v_2^*)^2}{r^*} + v_2^* = \frac{dp_2^*}{dr^*} \tag{2.19}$$

$$\frac{(v_3^*)^2}{r^*} + v_3^* = \frac{dp_2^*}{dr^*} + 3\frac{d\eta^*}{dr^*} \tag{2.20}$$

$$\frac{1}{r^*}\frac{d}{dr^*}(r^* v_2^*) = -\eta^* \tag{2.21}$$

$$\frac{1}{r^*}\frac{d}{dr^*}(r^* v_3^*) = \eta^* \tag{2.22}$$

(b) *Boundary conditions*

Since there is divergence in all layers (i.e. in the lens as well as the fluid above and below), a velocity field must exist in them which satisfies,

$$v_1^* = v_2^* = v_3^* = 0;\ r^* = 0. \tag{2.23}$$

The second boundary condition is, of course, that the orbital velocity must also vanish at infinity,

$$v_1^* = v_2^* = v_3^* = 0;\ r^* \to = \infty. \tag{2.24}$$

(c) *Solution*

First, it is recalled that for $\varepsilon \to$ O (i.e. the basic state) the lens degenerates to a point. Hence, the solution is,

$$\left.\begin{aligned} v_1^* &= -fr^*/2 \\ h_1^* &= -(r^*)^2/8 \\ \zeta_1 &= -(r^*)^2/16 \\ v_2^* &= p_2^* = v_3^* = p_3^* = 0 \\ \eta^* &= 0 \end{aligned}\right\} \quad \varepsilon = 0. \tag{2.25}$$

We now proceed by assuming that the general solution possesses the expansions,

$$\left.\begin{aligned} h_1^* &= -(r^*)^2/8 + \varepsilon h_1^{(1)} + \varepsilon^{3/2} h_1^{(2)} + \varepsilon^2 h_1^{(3)} + \cdots \\ \xi_1^* &= -(r^*)^2/16 + \varepsilon \xi_1^{(1)} + \varepsilon^{3/2} \xi_1^{(2)} + \varepsilon^2 \xi_1^{(3)} + \cdots \\ v_2^* &= \varepsilon^{3/2} v_2^{(3)} + \varepsilon^2 v_2^{(4)} + \cdots \\ v_3^* &= \varepsilon^{3/2} v_3^{(3)} + \varepsilon^2 v_3^{(4)} + \cdots \\ p_2^* &= \varepsilon^2 p_2^{(4)} + \varepsilon^{5/2} p_2^{(5)} + \cdots \\ p_3^* &= \varepsilon^2 p_3^{(4)} + \varepsilon^{5/2} p_2^{(5)} + \cdots \\ \eta^* &= \varepsilon^2 \eta^{(4)} + \varepsilon^{5/2} \eta^{(5)} + \cdots . \end{aligned}\right\} \tag{2.26}$$

Note that the inclusion of the lens solution in the expansion is necessary (even though the

radius of the lens goes to zero) because the zeroth order expansion needs to satisfy the governing equation of the *three* layers.

Substitution of (2.26) into (2.14–2.22) and introducing the appropriate scale for the radius,

$$r^* = \varepsilon^{1/2}\hat{r} \tag{2.27}$$

gives, to leading order,

$$\left.\begin{aligned}
v_2^{(3)} &= \frac{\mathrm{d}p_2^{(4)}}{\mathrm{d}\hat{r}} && (2.28)\\
\frac{1}{\hat{r}}\frac{\mathrm{d}}{\mathrm{d}\hat{r}}(\hat{r}v_2^{(3)}) &= \frac{(\hat{r})^2}{16} - \xi_1^{(1)} && (2.29)\\
\frac{\mathrm{d}\xi_1^{(1)}}{\mathrm{d}\hat{r}} &= 0 && (2.30)\\
2\xi_1^{(1)} &= h_1^{(1)} && (2.31)\\
\frac{1}{\hat{r}}\frac{\mathrm{d}}{\mathrm{d}\hat{r}}(\hat{r}v_3^{(3)}) &= \frac{(\hat{r})^2}{8} - h_1^{(1)} && (2.32)
\end{aligned}\right\} \quad r \le R$$

$$\left.\begin{aligned}
v_2^{(3)} &= \frac{\mathrm{d}p_2^{(4)}}{\mathrm{d}\hat{r}} && (2.33)\\
v_3^{(3)} &= \frac{\mathrm{d}p_2^{(4)}}{\mathrm{d}\hat{r}} + 3\frac{\mathrm{d}\eta_2^{(4)}}{\mathrm{d}\hat{r}} && (2.34)\\
\frac{1}{\hat{r}}\frac{\mathrm{d}}{\mathrm{d}\hat{r}}(\hat{r}v_2^{(3)}) &= 0 && (2.35)\\
\frac{1}{\hat{r}}\frac{\mathrm{d}}{\mathrm{d}\hat{r}}(\hat{r}v_3^{(3)}) &= 0 && (2.36)
\end{aligned}\right\} \quad r \ge R.$$

The solution for the lens and the fluid directly above and below ($r \le R$) is easily found to be,

$$\xi_1^{(1)} = \mathrm{A};\ h^{(1)} = 2\mathrm{A} \tag{2.37}$$

$$v_3^{(3)} = \frac{\hat{r}^3}{64} - \frac{\mathrm{A}\hat{r}}{2} \tag{2.38}$$

$$v_3^{(3)} = \frac{\hat{r}^3}{32} - \mathrm{A}\hat{r} \tag{2.39}$$

$$p_2^{(4)} = \frac{\hat{r}^4}{256} - \frac{\mathrm{A}\hat{r}^2}{4} + p_0, \tag{2.40}$$

where the boundary condition (2.23) is satisfied, p_0 is the pressure under the lid at $r = 0$, and the constant A is found to be,

$$A = 1/16, \tag{2.41}$$

where the condition $\xi_1^*(\hat{r} = 1) = 0$ to $O(\varepsilon^2)$ has been used. Outside the lens ($\hat{r} \geq 1$) the solution is

$$v_3^{(3)} = 2v_2^{(3)} = \frac{B}{\hat{r}} \tag{2.42}$$

$$p_2^{(4)} = \tfrac{1}{2}B\ell n\,\hat{r} + C \tag{2.43}$$

$$\eta^{(4)} = \frac{B}{6}\ell n\,\hat{r} + D, \tag{2.44}$$

where the constants B, C and D are to be determined from the matching conditions at the edge of lens ($\hat{r} = 1$) where the velocity, pressures and depths must be continuous. One finds,

$$B = -\frac{1}{32}; \quad C = -\frac{3}{256} + p_0. \tag{2.45}$$

It can be shown that D is determined at higher order which, while possible, is not discussed here in the interest of brevity.

For the lens and the fluid above and below ($r \leq R$) our complete solution can now be written as,

$$h_1^* = \frac{\varepsilon}{8}(1 - \hat{r}^2) + O(\varepsilon^{3/2}) + \cdots \tag{2.46}$$

$$\xi_1^* = \frac{\varepsilon}{16}(1 - \hat{r}^2) + O(\varepsilon^{3/2}) + \cdots \tag{2.47}$$

$$v_1^* = -\varepsilon^{1/2}\frac{\hat{r}}{2} \tag{2.48}$$

$$v_2^* = -\varepsilon^{3/2}\frac{\hat{r}}{32}\left(1 - \frac{\hat{r}^2}{2}\right) + O(\varepsilon^2) + \cdots \tag{2.49}$$

$$v_3^* = -\varepsilon^{3/2}\frac{\hat{r}}{16}\left(1 - \frac{\hat{r}^2}{2}\right) + O(\varepsilon^2) + \cdots \tag{2.50}$$

$$p_2^* = \varepsilon^2\left(\frac{\hat{r}^4}{256} - \frac{\hat{r}^2}{64} + p_0\right) + O(\varepsilon^{5/2}) + \cdots. \tag{2.51}$$

Outside the lens ($r \geq R$), the solution is,

$$v_2^* = -\frac{\varepsilon^{3/2}}{64\hat{r}} + O(\varepsilon^2) + \cdots \tag{2.52}$$

$$v_3^* = -\frac{\varepsilon^{3/2}}{32\hat{r}} + O(\varepsilon^2) + \cdots \tag{2.53}$$

$$p_2^* = \varepsilon^2\left(-\frac{1}{64}\ln\hat{r} - \frac{3}{256} + p_0\right) + O(\varepsilon^{5/2}) + \cdots \tag{2.54}$$

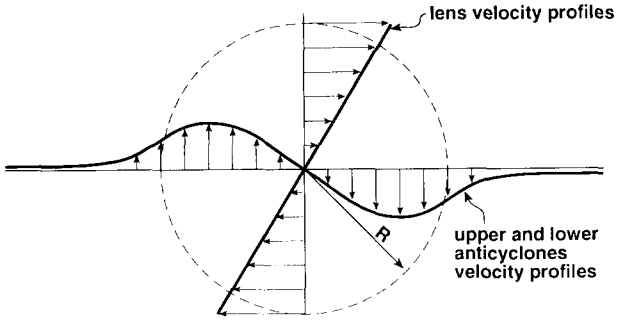

Fig. 4. Schematic diagram of the velocity profile in the laboratory lens and the weak anticyclones above and below. Note that (i) the orbital speed in the anticyclones above and below reaches its maximum at $r = (2/3)^{1/2}R$, and (ii) the velocity of these conjugate eddies extends beyond the lens boundary (see text).

$$\eta^* = O(\varepsilon^2) + \cdots. \tag{2.55}$$

Our general laboratory flow field can now be described as follows. Within the lens there are relatively strong flows and the velocity profile is identical to that of a solid body rotation. There are also relatively weak anticyclonic circulations both above and below the lens (see Fig. 4). These environmental circulations extend *beyond* the boundary of the lens; they decay as $1/r$. Even though these flows are small, they are important because they imply that the lenses start interacting with each other well *before* their edges meet. Note that in this sense the present laboratory experiments are very different from those of NOF and SIMON (1987) where, due to a different formation process, there were no flows outside the lens boundary. (However, the lenses in the numerical experiments discussed in Section 4 will have no comparable external flow field.) Last, the length scale of our solution in appropriate to the fine scale of the lens deformation radius, which is much smaller than the environmental deformation radius (cf. 2.11). Thus, the logarithmic behavior of p_2 in (2.54) represents the leading order behavior of the K_0 Bessel function for small argument. This can be understood by noting that the thermocline for $r > R$ adjusts to the presence of the lens on the R_d length scale, and our expansion here captures only the behavior near the lens.

Finally, it should be pointed out that the center of gravity of a zero-potential vorticity lens is located at a height of $\hat{h}/4$, where $\hat{h}$ is the central lens thickness (at $r = 0$). This implies that the center of gravity of the lens shown in Fig. 3 is situated one twelfth of the *total* lens thickness *above* the undisturbed interface. Similarly, a lens with a density of $(\rho + \Delta\rho)$ will have its center of gravity situated at one twelfth of its total thickness *below* the undisturbed interface.

3. EXPERIMENTS ON A ROTATING TABLE

(a) *Procedures*

To eliminate the possibility of air friction, the test container was covered with a clear flat Plexiglass plate (Fig. 2). Note, however, that since the movements of the lenses are relatively fast, it is doubtful that air friction could cause any difficulties. Before the

experiments were performed, the basin was leveled to within 30 s of an arc and centered to less than ± 1 mm of the table rotation axis. The 45 cm container was illuminated from above with a circular neon lamp. Two 35 mm motor driven cameras were used; one was mounted on the rotating table above the apparatus and took photographs from the top whereas the other was fixed to the stationary floor and took photographs from the side. The salty dyed eddies were injected (at a rate of 3 $cm^3 s^{-1}$) by gravity via two tubes (each situated 6 cm away from the center) connected to small reservoirs situated about 1 m above the tank. Two cylinders made of permeable foam with a diameter of 3 cm and a length of 2 cm were placed at the end of the injection tubes.

Before the experiment began, the tank was filled with salty water (whose density was 1.024 g cm^{-3}) to a depth of about 11 cm and fresh water was slowly poured from the top again via a permeable foam. After the top layer also reached a depth of about 11 cm, the tank was rotated counterclockwise at a uniform rate ($f = 2\Omega = 4\pi/T = 4.2\ s^{-1}$, where Ω is the rotation rate and T is the rotation period), until the system reached a solid body rotation (about 30 min). The experiments then began with a simultaneous release of the dyed salty water (with densities of 1.016 g cm^{-3} and 1.008 g cm^{-3}). Each tube constantly supplied 3 $cm^3 s^{-1}$ of lenses of water throughout the entire interaction process.

(b) *Results and analysis*

Side and top photographs of a "typical" experiment are shown in chronological order in Figs 5 and 6. An alignment of the lenses is clearly evident in the photographs; a schematic diagram of the alignment is shown in Fig. 7. By and large, the alignment occurred within 60–100 s, i.e. within 20–30 revolutions of the table. This alignment time is relatively long compared to the lenses orbital time scale (comparable to the table rotation rate). In that sense alignment is not much different from merging which has also been observed to be long compared to the orbital period (Cushman-Roisin and Tang, 1990; Nof and Simon, 1987).

Note, however, that, in our environmental fluid, which contains only two layers, the vertical separation between the lenses' center of gravity is limited; for our choice of densities and potential vorticity, it equals one sixth of a single lens thickness. In contrast, a continuously stratified ocean could contain lenses that have much greater vertical separation. This could, presumably, reduce the tendency to align.

The interaction between the two lenses begins immediately after their formation mainly due to the anticyclones above and below (Section 2) which extend much beyond the lens boundary. It is because of this interaction that the lenses in Fig. 5a and b are mutually advected in a clockwise manner even before their edges meet. In terms of the system energetics, the role of the anticyclones above and below is probably limited because, as the analysis in Section 2 demonstrates, the magnitude of the flows in the external anticyclones is very weak. This does not necessarily mean, however, that the environmental anticyclones are not playing any role in the actual alignment process here; it is quite possible that they can influence the interaction. With our simplified "kitchen type" laboratory experiments, the presence of the anticyclones is required and their role cannot be unambiguously assessed. However, the numerical experiments that follow argue that the environmental anticyclones are not *required* for alignment to occur.

Note that, strictly speaking, the solution presented in Section 2 can be applied to our laboratory experiment only for a "window" of time, beginning when the lens growth rate

becomes small enough and ending when the lens depth becomes comparable to the tank depth. This time window covers most of the period shown in Figs 5 and 6. It is clear from all of the photographs that, in a similar fashion to the case of eddy merging, filamentation is an integral part of the alignment. As pointed out by CUSHMAN-ROISIN (1989), and as can be shown here, filamentation is necessary because (i) a fraction of the lenses mass must be expelled in order to allow energy conservation, and (ii) as the two lenses are drawn closer to each other, the total angular momentum decreases so that some fluid must be ejected to compensate for it. Details are excluded in the interest of brevity.

4. NUMERICAL EXPERIMENTS

The purposes of our numerical study were to provide experiments for qualitative comparison with the laboratory results, and to examine details of the alignment in an environment that is easily controlled and that can be modeled after the actual ocean. As such, no detailed attention will be given here to the classical question of the critical separation distance beyond which alignment does not occur. We will, however, make relevant comments at the appropriate points.

The results of a "typical" numerical alignment experiment are shown in Fig. 8. The upper panels in Fig. 8 are of a second layer thickness and the lower layer panels are of third layer thickness. Results from days 0, 2, 6, 8 and 18 are shown.

The initial profile demonstrates that these eddies were weakly in contact. Again, the decay scale of both Gaussian profiles was 25 km, and the initial eddy separation (i.e. distance between maximum thicknesses) was 64 km. (We mention that in an experiment with an initial separation of 80 km, the eddies did not "align"; more on this later.) The sequence of diagrams demonstrates that alignment occurs; by day 18, the eddies are approximately circular and horizontally coincident. Subsequent evolution is very slow, so that the alignment process can be considered as complete by day 18. As a point of reference, the minimum eddy circulation time is roughly one day. Thus these experiments are in agreement with the time scales suggested by the laboratory; namely, that alignment requires a relatively long span of time to occur ($\sim$20 circulation time scales).

The mechanics of alignment appear in these figures. The radial symmetry of each individual vortex profile is broken by their mutual overlap. As a result, inertial effects cause a significant distortion in the eddies' profiles. This happens relatively quickly (i.e. on the circulation time scale) so that by day 2 of our experiment ($\sim$ 2 turnover times, see Fig. 8b), the eddies are clearly wrapping around each other. Again, this is consistent with the laboratory results.

Figure 9 contains a plot of the separation between the eddy maximum thicknesses versus time during the interaction. The above short term tendencies towards alignment appear in the initial decrease of the separation distance, which begins at roughly hour 50 of the experiment. What is very interesting is that the temporal difference between the alignment time scales and the vortex circulation time scales is resolved by this plot. Note that the separation distance approaches a minimum by hour 120, but then begins a dramatic increase towards a maximum.

This secondary maximum obtains a value of $\sim$ 60 km, which is virtually indistinguishable from the initial vortex separation distance, at hour 200 (Fig. 8d). Following this, separation distance again oscillates in magnitude one more cycle, and then changes markedly in character. The last phase of behaviour is marked by a capture of separation

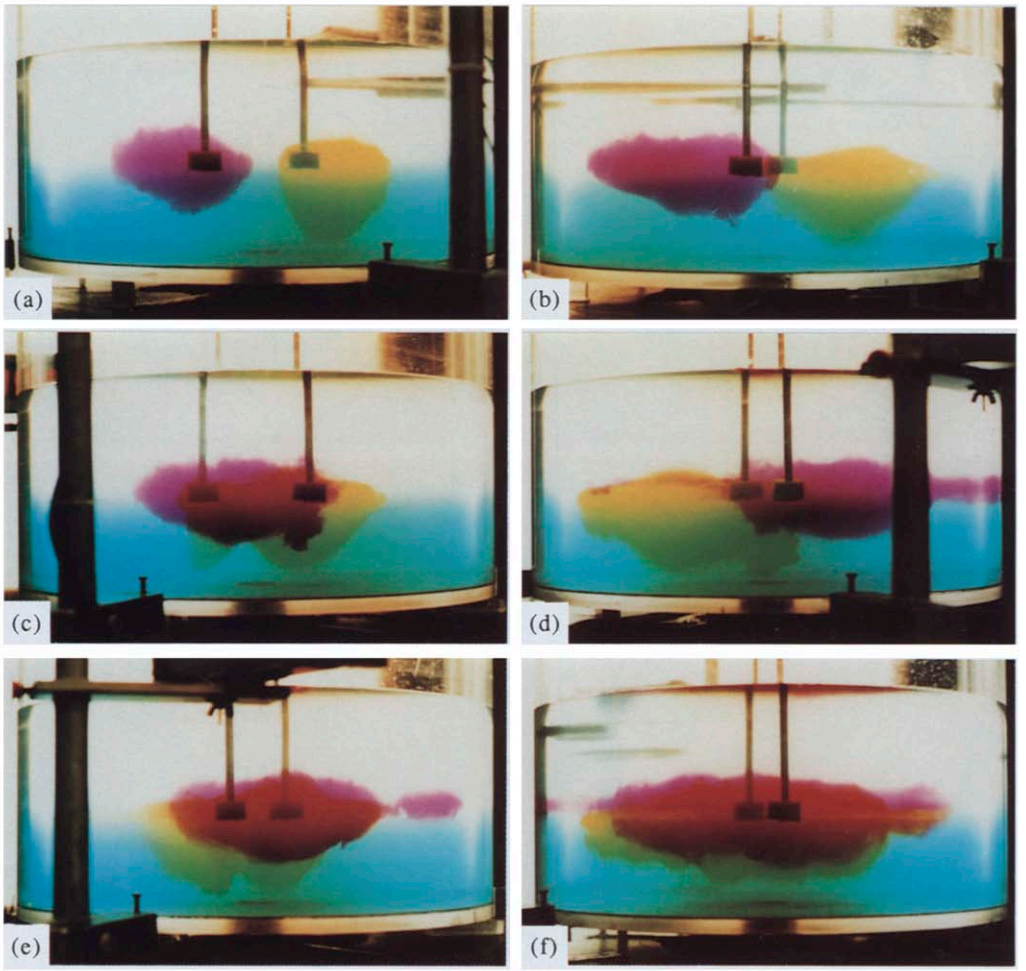

Fig. 5. Side photographs of the lenses during the various stages of their interaction and alignment. Note that fluid is constantly supplied through the vertical tubes (at a rate of 3 cm^3 s^{-1}) so that the lenses are constantly growing during the interaction process. The entire interaction lasted approximately 2 min with the consecutive photographs taken at intervals of approximately 25 s. The Coriolis parameter $f = 2\Omega = 4\pi/T$ (where Ω is the rotation rate and T is the period) was 4.2 s^{-1}. Note that, since the side camera was attached to the floor and did not rotate with the table, the relative positions from which the various photographs were taken are not identical.

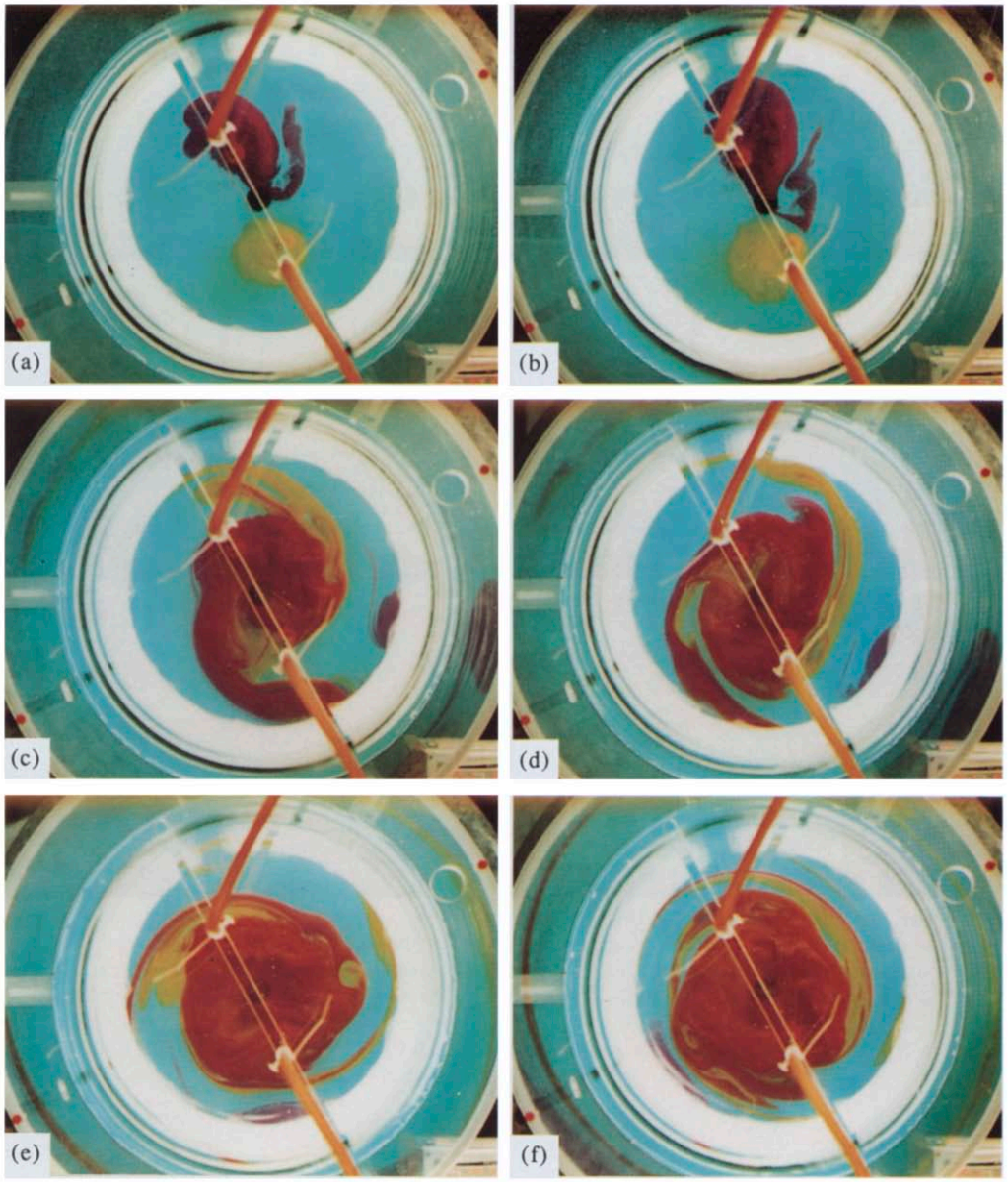

Fig. 6. Top photographs of the alignment process taken by a camera fixed to the table. Note that the time interval between two consecutive photographs is again approximately 25 s but each photograph does not necessarily correspond to the one shown from the side (i.e. there might be a mis-match of about 1–3 s). Because of the mutual interaction of the lenses as well as the interaction of the anticyclones above and underneath, the pair moves clockwise relative to the rotating tank. Since the lenses are constantly fed by new fluid, this causes the lenses to be somewhat asymmetrical. Note that the white circle in the middle of each photograph is the (unavoidable) reflection of the circular neon lamp illuminating the tank.

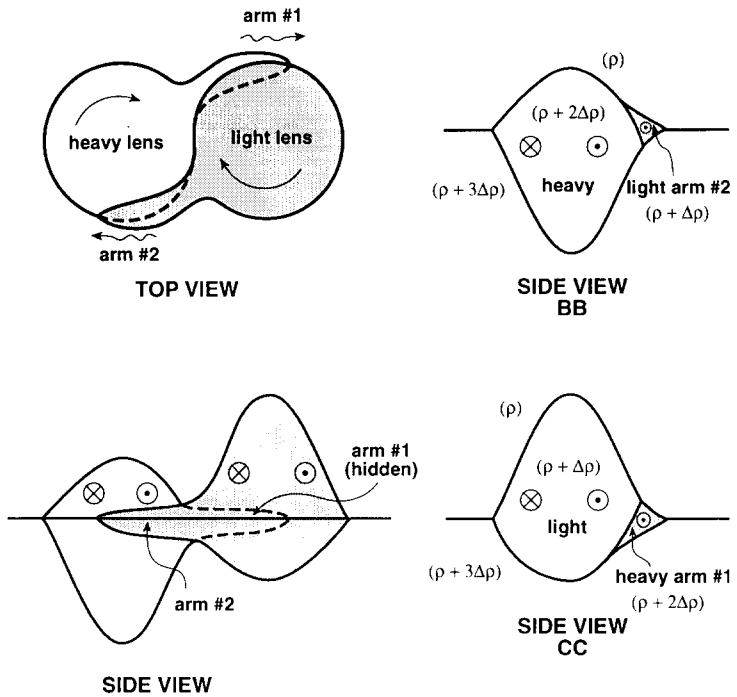

Fig. 7. Schematic diagram of the arms extended from one vortex to the other during the first stage of the alignment. The arm of the heavy lens (arm no. 1) dives partially under the light lens whereas the arm of the light lens (arm no. 2) partially floats on top of the heavy lens. Ultimately, all the lenses' fluid "leaks" via the arms and the final state consists of one lens on top of the other, i.e. the spiral configuration discussed by Nof (1988) for the merging of lenses with identical densities [shown in (his) Fig. 4b] is not established. "Wavy" arrows denote propagation.

distance at a small value, followed by a much slower reduction in magnitude. This last phase begins at roughly hour 400, and its structure is depicted in our sequence by Fig. 8e.

The numerical sequence clearly depicts the oscillations as a result of inertial mechanics. Specifically, the vortices by their interaction initially distort, so that on a circulation time scale they develop into highly asymmetrical structures (Fig. 8b). This is followed by an "overshoot", a reorganization of the eddies into roughly circular shapes, and a repeat of the above sequence. Considerable gravity wave activity is generated during this process, which results in a loss of energy by the eddies. Because of this, and because of the alignment process, the eddies' maximum thicknesses reduce during each of the oscillation phases (see Fig. 10).

Thus we have the result that the vortices' interaction time scale is set by the eddy circulation time, which is not terribly surprising. The question remains as to what determines the alignment time scale. This remains an open question, but we here mention that the time-scale is not a simple function of the nonlinearity. To demonstrate this, we show in Fig. 11 a plot of vortex separation versus time. The eddies in this experiment were characterized by maximum initial thicknesses of 250 m, i.e. amplitudes of roughly half those for the eddies in Fig. 8.

Clearly, the circulation times of these eddies are larger (by roughly a factor of 2) than

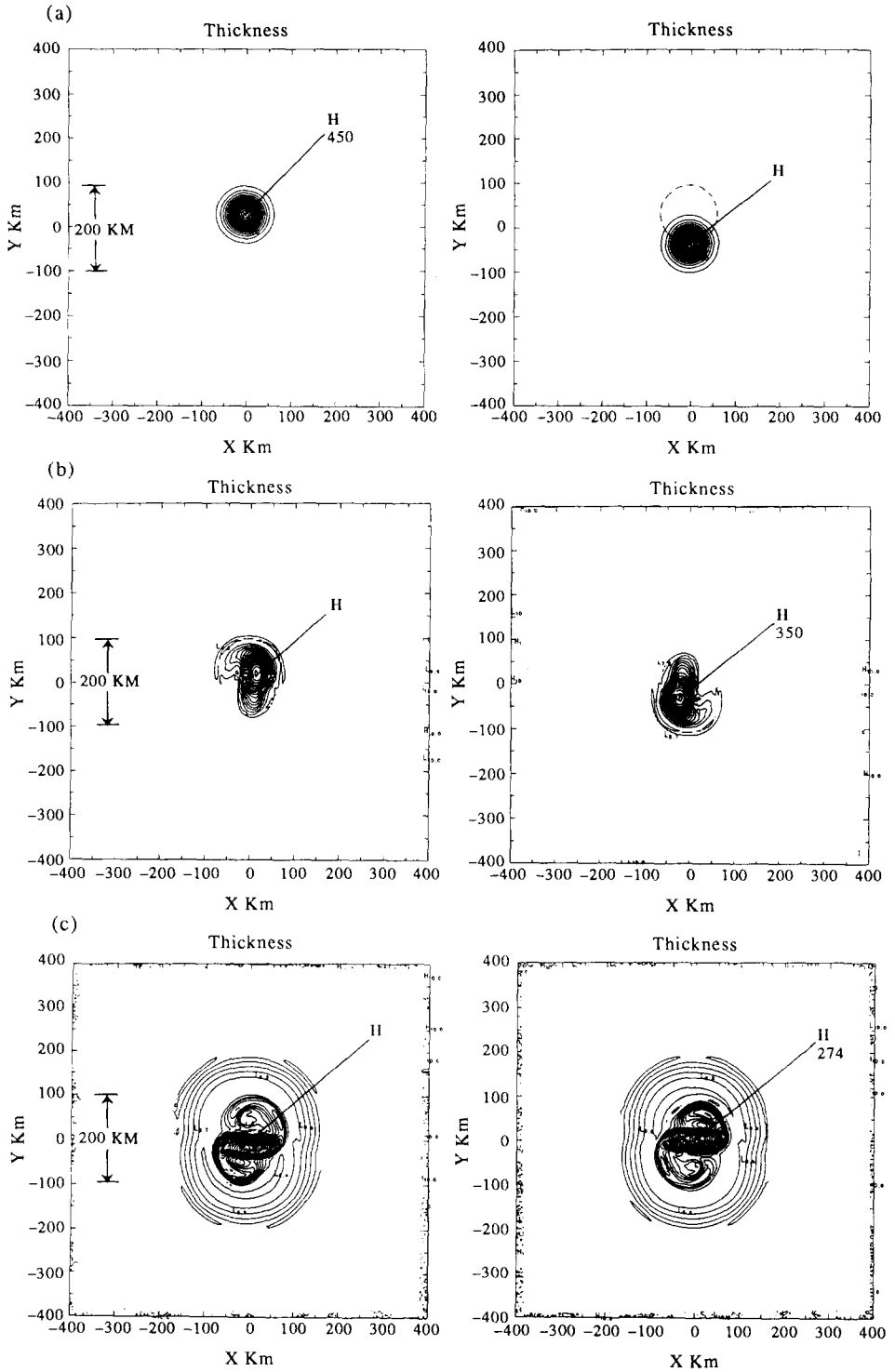
(a)
Thickness
H
450
200 KM
Y Km
X Km
Thickness
H
(b)
Thickness
H
200 KM
Y Km
X Km
Thickness
H
350
(c)
Thickness
H
200 KM
Y Km
X Km
Thickness
H
274

Fig. 8.

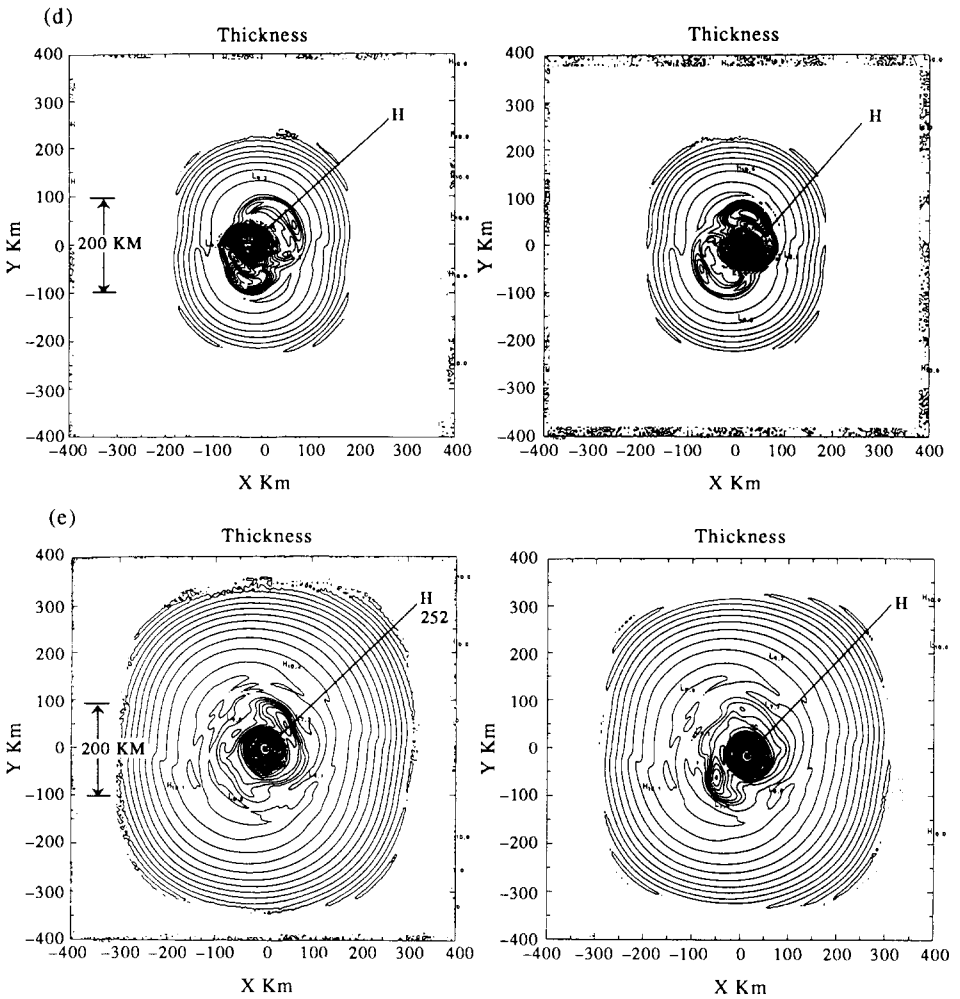

Fig. 8. Numerical alignment-thickness. Initial layer 2 thickness appears in the upper panels and layer 3 thickness in the lower panels. The lenses' centers are off-set by a distance of 64 km. The initial location of the upper lens relative to the lower lens appears in (a) as the dashed line, which represents the 25 m contour. Days 0, 2, 6, 8 and 18 are shown in (a), (b), (c), (d) and (e), respectively (CI = 25 m, 20 m, 10 m, 10 m, 10 m, also respectively). Note the distortion and arm production in (b), (c) and (d). Alignment is effectively completed by day 18, which is roughly 20 circulation times.

those of our previous experiment. One might, therefore, expect that total alignment time might be twice that (~800 h) of the earlier results. Figure 11 demonstrates, however, that alignment occurs roughly at hour 550, and further that quantitative differences exist between these and the earlier results. Most notably, the number of oscillations have decreased from 3 to 2, with the second oscillation much weaker in amplitude than the first. The time scales of these oscillations still coincide with the eddy turnover time, as they did for our previous experiment.

Thus, we conclude that the alignment time scale is a weak function of vortex nonlinear-

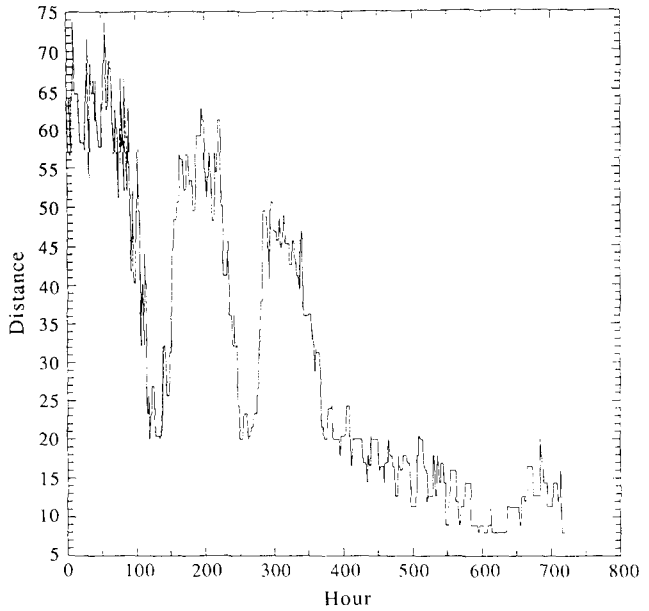

Fig. 9. Separation distance versus time for the lenses shown in Fig. 8. The eddies' centers were initially 64 km apart. Note the oscillations, consistent with an inertial "overshoot" of the eddies, and that the vortices are eventually captured by hour 400.

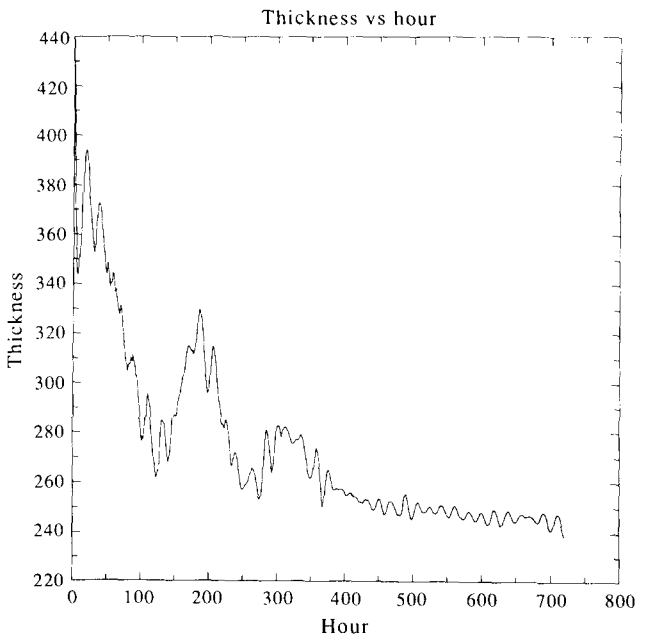

Fig. 10. Second layer vortex maximum thickness versus time. These results come from the previous eddy experiment. Note the loss in amplitude, occurring jointly due to the alignment process and the loss in energy to the gravity wave field.

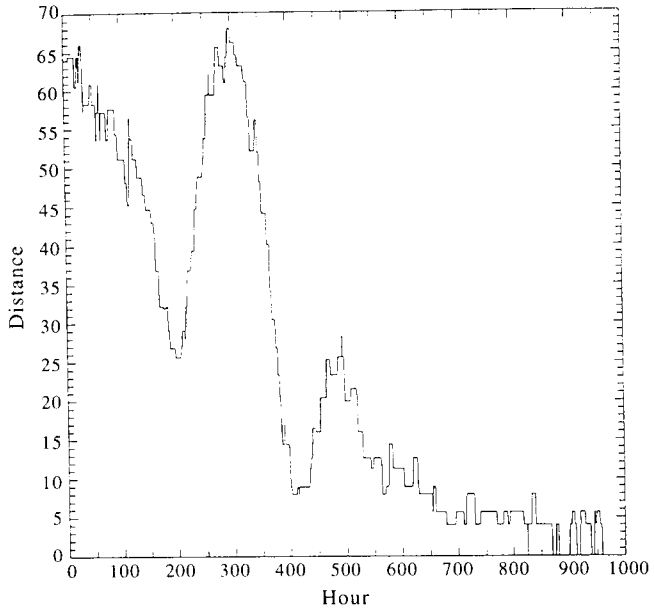

Fig. 11. Separation distance versus time for weak lenses. Here, the eddy initial amplitude was half that of the previous experiment. The inertial overshoots again occur, but are slower in occurrence and fewer in number. Nonetheless, vortex alignment, occurring roughly at hour 550, does not require a very different amount of time to occur relative to the stronger eddy. Hence, alignment time appears to be a weak function of nonlinearity.

ity. We speculate that this is due to two competing influences introduced by eddy nonlinearity. The first is the obvious idea that highly nonlinear eddies will have strong tendencies to align, due to their stronger circulation. The second competing effect, however, is that stronger baroclinic eddies have stronger isopycnal perturbations associated with them. Vertical alignment, which requires a considerable distortion in the structure of the initially isolated eddies, therefore should be somewhat resisted by nonlinear eddies due to their structural integrity. The result in the present experiments is that these competing effects can roughly offset each other, so that the alignment time scales are not very different, even though the participant eddies are structurally very different.

Finally, a word about the critical separation issue is in order. It appears that the critical distance is a complicated function of eddy nonlinearity. In quasi-geostrophic theory, this distance is essentially set by the environmental baroclinic deformation radius,

$$d_c = R_d = \frac{\alpha[g'H_1]^{1/2}}{f_0},$$

where α often obtains a value of ~3 [see, for example, the $\Gamma = 1$ results of POLVANI (1991)]. In our numerical experiments, $R_d \sim 50$ km, but as mentioned earlier, complete alignment did not occur for a separation of 80 km (< 150 km $\sim \alpha R_d$).

The other possibly relevant length scale in this problem is the deformation radius based on the lens density anomaly. Again, for the experiment in Fig. 8, this is roughly $R_{df} = 25$

km, suggesting that the above critical α value multiplying $R_{d\ell}$, might substitute effectively here for the critical separation criteria. On the other hand, Fig. 11 demonstrates an alignment of two eddies with $h_m = 250$ m, for which $R_{d\ell} \sim 18$ km. The initial lens separation here was 64 km, which exceeds the above *ad-hoc* critical distance, but the lenses clearly merged.

In a few other experiments in the quasi-geostrophic range ($\delta h \sim 20$ m), eddies initially separated by 64 km aligned quite effectively. This, of course, is in keeping with quasi-geostrophic expectations.

In summary then, it appears that the general critical separation distance criterion for eddies is a function of both the environmental and lens deformation radii. The latter dependence represents an extension of the existing quasi-geostrophically determined dependencies, which do not allow for finite amplitude thickness variations. In between these limiting cases, some dependence on both length scales may well exist; we stress that we have not determined these dependencies here.

To complicate the story even more, the lenses which failed to align completely (i.e. the lenses separated initially by 80 km), did exchange some mass. However, the amount of mass was small, and after 14 days of interaction, two distinct lenses remained. Further, these lenses were only very weakly interacting.

Clearly, much work remains to be done to clarify the question of alignment and critical separation for nonlinear lenses. We hope the qualitative results presented here will provide useful information to guide future studies.

5. SUMMARY

We find that alignment is a relatively slow process for nonlinear eddies, in that it requires several turnover times. This is consistent with eddy merger studies, where eddies of equal density were studied. The alignment process involves the generation of arms which encircle these interactive eddies. The numerical experiments demonstrate that the arms are the result of inertial mechanics and distortion. Further, the eddies have a tendency to oscillate about one another prior to final unification. Streamers are shed by the eddies as a result of angular momentum considerations. A somewhat unexpected result is that the alignment time scale is a weak function of nonlinearity. This appears to be due to the competing influences of vortex thickness, which tends to resist alignment, and circulation strength, which tends to speed up interaction.

Thus our results extend existing studies of vortex interaction into the regime of nonlinear eddies and demonstrate the capacity for such eddies to align. Given that many eddies are generated in relatively confined areas (e.g. warm eddies in the Slope Water and Meddies in the Mediterranean outflow region), like-signed vortex interaction should be a relatively commonplace occurrence. The results contained herein should therefore find application to the interpretation of vortex observations.

Acknowledgements—We thank Mr Sergey Borisov for executing and photographing many of the laboratory experiments. Comments by J. McWilliams and W. Zenk on an earlier version of this article were very useful. This study was supported by Office of Naval Research grants N00014-89-J-1577 and N00014-89-J-1606, by National Science Foundation grants OCE-9012114 and OCE-9102025, and by NASA grant NAGW-3087.

REFERENCES

AMBAR I., L. ARMI, M. O. BARINGER, A. BOWER, A. FIÚZA, G. C. JOHNSON, R. KÄSE, M. KENNELLY, E. KUNZE, R. LUECK, P. LUNDBERG, C. G. MARTINS, M. D. PRATER, J. PRICE, M. RHEIN, T. SANFORD, K. TOKOS, J.

VERRALL and W. ZENK (1992) In *Proc. Intl. Workshop on Outflows and Overflows in the Atlantic and Their Role in the Eastern Boundary Current System*. University of Lisbon, Portugal, 1991.

ARMI L., D. HEBERT, N. OAKEY, J. F. PRICE, P. L. RICHARDSON, H. T. ROSSBY and B. RUDDICK (1989) Two years in the life of a Mediterranean salt lens. *Journal of Physical Oceanography*, **19**, 354–370.

BLECK R. and D. BOUDRA (1986) Wind-drive spin-up in eddy-resolving ocean models formulated in isopycnic and isobaric coordinates. *Journal of Geophysical Research*, **91**, 7611–7621.

CHASSIGNET E. and B. CUSHMAN-ROISIN (1991) On the influence of a lower layer on the propagation of nonlinear oceanic eddies. *Journal of Physical Oceanography*, **21**, 939–957.

CRESSWELL G. R. (1982) The coalescence of two East Australian Current warm-core eddies. *Science*, **215**, 161–164.

CRESSWELL G. R. and R. LEGECKIS (1987) Eddies off southeastern Australia, 1980/91. *Deep-Sea Research*, **34**, 1527–1562.

CUSHMAN-ROISIN B. (1989) On the role of filamentation in the merging of anticyclonic lenses. *Journal of Physical Oceanography*, **19**, 253–258.

CUSHMAN-ROISIN B. and B. TANG (1990) Geostrophic turbulence and emergence of eddies beyond the radius of deformation. *Journal of Physical Oceanography*, **20**, 97–113.

DEWAR W. K. and C. GAILLIARD (1993) The dynamics of barotropical dominated rings. *Journal of Physical Oceanography*, **24**, 5–29.

DEWAR W. K. and P. K. KILLWORTH (1990) On the cylinder collapse problem, mixing and the merger of isolated eddies. *Journal of Physical Oceanography*, **20**, 1563–1575.

GILL A. E. (1981) Homogeneous intrusions in a rotating stratified fluid. *Journal of Fluid Mechanics*, **103**, 275–295.

GILL A. E. and R. W. GRIFFITHS (1981) Why should two anticyclonic eddies merge? *Ocean Modelling*, **41**, 10–16.

GRIFFITHS R. W. and E. J. HOPFINGER (1986) Experiments with baroclinic vortex pairs in a rotating fluid. *Journal of Fluid Mechanics*, **173**, 501–518.

GRIFFITHS R. W. and E. J. HOPFINGER (1987) Coalescing of geostrophic vortices. *Journal of Fluid Mechanics*, **178**, 73–97.

MASINA S. and N. PINARDI (1993) The halting effect of baroclinicity in vortex merging. *Journal of Physical Oceanography*, **23**, 1618–1637.

MCWILLIAMS J. (1989) Statistical properties of decaying geostrophic turbulence. *Journal of Fluid Mechanics*, **198**, 199–230.

MCWILLIAMS J. and N. ZABUSKY (1982) Interactions of isolated vortices. I: Modons colliding with modons. *Geophysical and Astrophysical Fluid Dynamics*, **19**, 207–227.

MELANDER M. V., N. J. ZABUSKY and J. C. MCWILLIAMS (1985) A model for symmetric vortex-merger. *Transactions of the Third Army Conference on Applied Mathematics and Computing, ARO Report* 86-1.

MELANDER M. V., J. C. MCWILLIAMS and N. J. ZABUSKY (1987) Axisymmetrization and vorticity-gradient intensification of an isolated two-dimensional vortex through filamentation. *Journal of Fluid Mechanics*, **178**, 137–159.

MELANDER M. V., N. J. ZABUSKY and J. C. MCWILLIAMS (1988) Symmetric vortex merger in two dimensions: Causes and conditions. *Journal of Fluid Mechanics*, **195**, 303–340.

NOF D. (1988) The fusion of isolated nonlinear eddies. *Journal of Physical Oceanography*, **18**, 887–905.

NOF D. and L. SIMON (1987) Laboratory experiments on the merging of anticyclonic eddies. *Journal of Physical Oceanography*, **17**, 343–357.

POLVANI L. M., N. J. ZABUSKY and G. R. FLIERL (1989) Two-layer geostrophic vortex dynamics. Part 1. Upper-layer V-states and merger. *Journal of Fluid Mechanics*, **205**, 215–242.

POLVANI L. M. (1991) Two-layer geostrophic vortex dynamics. Part 2. Alignment and two-layer V-states. *Journal of Fluid Mechanics*, **225**, 241–270.

RICHARDSON P. L., D. WALSH, L. ARMI, M. SCHRÖDER and J. F. PRICE (1989) Tracking three Meddies with SOFAR floats. *Journal of Physical Oceanography*, **19**, 371–383.

ROBINSON A. R., J. A. CARTON, N. PINARDI and C. N. K. MOOERS (1986) Dynamics forecasting and dynamics interpolation: an experiment in the California Currents. *Journal of Physical Oceanography*, **16**, 1561–1579.